

Inverse-feedforward of charge-controlled piezopositioners ^{☆,☆☆}

G.M. Clayton ^{a,*}, S. Tien ^a, A.J. Fleming ^b, S.O.R. Moheimani ^b, S. Devasia ^a

^a Department of Mechanical Engineering, University of Washington, Box 352600, Seattle, WA 98195, USA

^b School of Electrical Engineering and Computer Science, University of Newcastle, University Drive, Callaghan, NSW 2308, Australia

Abstract

Inverse-feedforward control can substantially improve the performance of piezoelectric positioners (piezopositioners). The feedforward-input is found by modeling and inverting the piezopositioner dynamics. The primary challenge in such an approach is the complexity of modeling and inverting the hysteresis nonlinearity in the piezopositioner dynamics. The main contribution of this work is to alleviate this complexity by using charge control to linearize the overall dynamics and then model and invert the simplified (linearized) dynamics. The proposed approach is applied to an experimental piezopositioner and results are presented to contrast the feedforward-based positioning performance with and without the use of charge control to linearize the dynamics.

© 2007 Elsevier Ltd. All rights reserved.

Keywords: Piezopositioners; Charge control; Inverse-feedforward; Hysteresis; Vibrations

1. Introduction

Inverse-feedforward control can substantially improve the performance of piezoelectric positioners (piezopositioners) [1–3] that are widely used in mechatronic systems, e.g., scanning probe microscopy (SPM) [4] and SPM-based nanofabrication [5]. The feedforward-input is found by modeling and inverting the piezopositioner dynamics [1], and can then be applied to the system to improve the piezopositioner performance. Typically feedforward is integrated with feedback; the addition of feedforward to feedback tends to improve the positioning performance when compared to the performance of feedback alone [2]. The primary challenge in such an approach is the complexity of modeling and inverting the hysteresis nonlinearity in the piezopositioner dynamics. The main contribution of this work is to alleviate this complexity by using charge

control to linearize the overall dynamics [6,7] and then model and invert the simplified (linearized) dynamics. The proposed approach is applied to an experimental piezopositioner and results are presented to contrast the feedforward-based positioning performance with and without the use of charge control to linearize the piezopositioner dynamics.

The complexity of modeling and inverting the hysteresis nonlinearity is the main challenge in computing the feedforward-input for piezopositioners. A typical inverse-feedforward computation is shown in Fig. 1 – note that both the linear dynamics (G – vibrations and creep) and the hysteresis nonlinearity (H) are inverted to find the feedforward-input (u_{ff}), which is then applied to the piezopositioner as a feedforward-input ($v_{in} = u_{ff}$). The hysteresis nonlinearity can be captured using different models such as the Preisach model [8–10], multiple linear-play (backlash) models [11,12], and deterministic path (polynomial) models [13]. These models can then be inverted (for example using iterative approaches [8,11]) to find the inverse-feedforward-input. An alternative method to modeling and then inverting, is to directly model the inverse hysteresis \hat{H}^{-1} [1,14] and use it to find the inverse-feedforward-input. Common to all these approaches is a

^{*} Portions of this article were published at The 4th IFAC Symposium on Mechatronics Systems under the title: Hysteresis and vibration compensation by integrating charge control and inverse-feedforward.

^{☆☆} This work was supported by NSF Grant CMS 0301787.

^{*} Corresponding author. Tel.: +1 206 885 3309.

E-mail address: gclayton@u.washington.edu (G.M. Clayton).

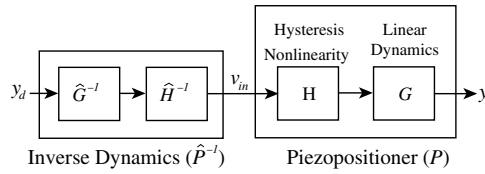


Fig. 1. Inverse-feedforward computation by inverting the piezopositioner dynamics P . Both the linear dynamics (G – vibrations and creep) and the hysteresis nonlinearity (H) are inverted to find the feedforward-input (u_{ff}), which is then applied to the piezopositioner as a feedforward-input ($v_{in} = u_{ff}$).

high-order model required to capture the hysteresis nonlinearity. An associated problem is that the parameters of such high-order hysteresis models tend to be sensitive to operating conditions such as temperature and aging effects. Therefore, the parameters of the model need to be frequently recalibrated and the feedforward-input needs to be frequently recomputed, which adds to the computational load. These computational challenges limit the use of inverse-feedforward in the presence of hysteresis nonlinearity.

We propose to first linearize the piezopositioner dynamics using charge control and then invert these simplified (linearized) dynamics to compute the inverse input as shown in Fig. 2. The use of a charge amplifier in cascade with the piezopositioner results in an overall linearized system (P_L). This linearized system can now be modeled (\hat{P}_L) and inverted (\hat{P}_L^{-1}) to compensate for the piezopositioner's dynamics. The inverse of the linearized system is relatively easy to compute and has been applied for precision positioning applications in previous works [14–16]. Thus, the main advantage of the approach is to circumvent the difficulties associated with inverting the hysteresis nonlinearity by using charge control as opposed to the typically used voltage control (without charge) [6]. It is noted that the hysteresis appears as an input nonlinearity between the applied voltage input and the induced charge – therefore, charge control can significantly reduce this input nonlinearity by up to 90% [7]. To show the effectiveness of this method, it is applied to control an experimental piezopositioner in Section 3. The experimental results show substantial reductions in the positioning error with the use of the proposed approach.

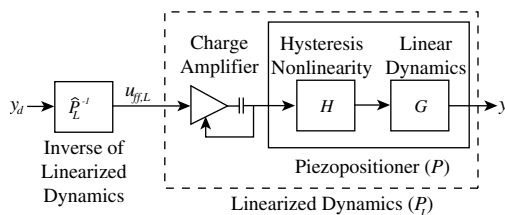


Fig. 2. Proposed approach computes the inverse input $u_{ff,L}$ by first linearizing the overall dynamics using charge control and then inverting the linearized dynamics \hat{P}_L .

The remainder of this article is organized as follows. The methods used in the article are described in Section 2. Experimental results are presented and discussed in Section 3. Section 4 presents our conclusions.

2. Methods

In this section, the components of the inverse-feedforward method shown in Fig. 2 are described, including the design of the charge amplifier, the experimental modeling of the linearized dynamics (\hat{P}_L), and the computation of the inverse-feedforward (\hat{P}_L^{-1}).

2.1. Charge amplifier

The charge amplifier linearizes the overall dynamics of the piezopositioner. Previous works have shown that operating piezopositioners with charge control, as opposed to voltage control, reduces the overall input nonlinearity by up to 90% [6,7]. This reduction in nonlinearity can be explained with a commonly used lumped parameter model of a piezopositioner [17,18], shown in Fig. 3, wherein the piezopositioner is modeled as the series combination of a voltage source (v_p , which is proportional to the piezopositioner strain), a capacitor (C_L , which captures the capacitance of the piezopositioner) and a nonlinear impedance (Δ , which models the hysteresis). It is noted that the deflection of the piezopositioner is proportional to the charge (q_{LC}) on the capacitor (C_L) [17].

When operated using a voltage amplifier, Fig. 3a, the charge on the capacitor (q_{LC}) is not linearly related to input voltage (v_{in}) because the voltage across the capacitor (v_{LC} – proportional to charge) is not linearly related to the input voltage (v_{in}) due to the nonlinear hysteresis element (Δ). Therefore, hysteresis is seen between the input voltage and output displacement.

In contrast, if a charge amplifier is used, Fig. 3b, then the input charge (q_{in}) collects on the capacitor (C_L) and is not effected by the nonlinear impedance (Δ). This results in a linear relationship between the input charge (q_{in}) and the charge on the capacitor (q_{LC}), and therefore, a linear relationship between the input charge and output displacement. Thus, the hysteresis nonlinearity can be avoided by driving the piezopositioner with a charge amplifier.

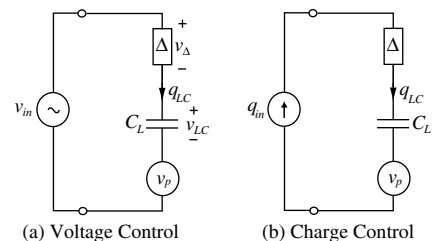


Fig. 3. Lumped parameter model of the piezopositioner: voltage amplifier and charge amplifier.

2.1.1. Low-frequency limitation of charge amplifiers

The application of charge amplifiers at low frequencies is limited by charge leakage, which can be modeled as a resistance (R_L) placed in parallel with the capacitor as shown in Fig. 4. To illustrate the loss of control at low-frequency, it is sufficient to consider a simplified model which neglects the nonlinear impedance (A) and the voltage (v_p) generated by the piezopositioner strain in Fig. 3.

Then, the relation between the input charge (q_{in}) and the charge on the capacitor (q_{LC}) can be obtained as

$$q_{LC}(s) = \frac{R_L C_L s}{R_L C_L s + 1} q_{in}(s), \quad (1)$$

which contains a high-pass filter with a cutoff frequency $\omega_c = \frac{1}{R_L C_L}$. This high-pass filter leads to poor low-frequency tracking and thus, the high-pass filter behavior precludes the use of charge amplifiers in applications requiring low-frequency positioning. Although the charge amplifier's performance is affected at low frequencies by the leakage resistance (R_L) in Fig. 4, the performance as a voltage amplifier is not affected by the leakage resistance since it is in parallel to the main piezopositioner capacitor.

2.1.2. DC-accurate charge amplifier

DC-accurate charge amplifiers [7,19] resolve the low-frequency limitations of typical charge amplifiers by operating as voltage amplifiers at low frequencies and as charge amplifiers at high frequencies. Although, this use of a voltage amplifier at low-frequency implies that hysteresis non-linearity is not compensated at low frequencies, such an approach avoids the high-pass behavior of traditional charge amplifiers. Moreover, low-frequency errors (including hysteresis) can be corrected with relative ease using standard integral-type feedback methods. Additional advantages of this approach such as the ability to drive grounded loads (e.g., typical piezopositioner configurations) are discussed in Ref. [7].

The circuit diagram for the DC-accurate charge amplifier is shown in Fig. 5, with the piezopositioner shown in gray. The high gain feedback amplifier (k_C) equates the applied reference voltage (v_{ref}), to the voltage (v_s) across a sensing capacitor (C_s). At high frequencies this circuit acts as a charge amplifier since the impedances of the capacitors are much smaller than the resistances at high frequencies. At low frequencies, the resistances are much smaller than

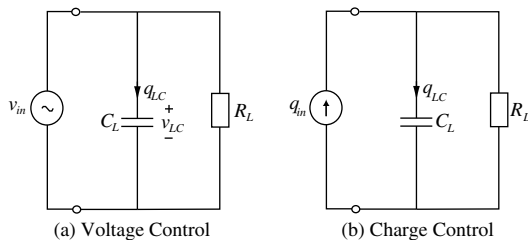


Fig. 4. Simplified lumped parameter model of the piezopositioner: voltage amplifier and charge amplifier with charge leakage modeled by resistance (R_L).

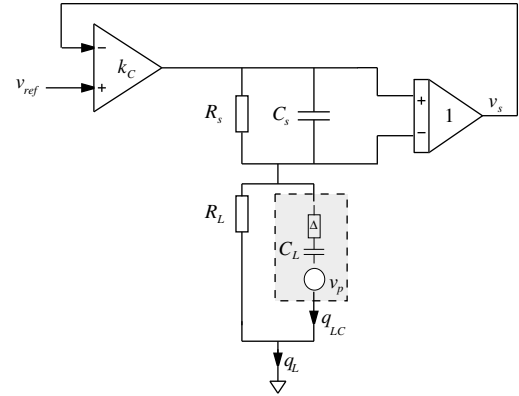


Fig. 5. DC-accurate charge amplifier [7].

the impedance of the capacitors and the circuit approximates a voltage amplifier. The crossover frequency (ω_c) between charge and voltage amplifier characteristics is $\omega_c = \frac{1}{C_s R_s}$; above ω_c the amplifier is charge dominant and below ω_c the amplifier is voltage dominant. Details of the amplifier design are discussed in Refs. [7,19].

2.2. Experimental modeling

The linearized dynamics (\hat{P}_L from Fig. 2) needed to find the inverse-feedforward were obtained experimentally using a dynamic signal analyzer (DSA) (Stanford Research Systems SR785). A swept-sine technique was used in which sinusoidal inputs of varying frequencies were applied by the DSA to the system and the resulting motion of the piezopositioner (the output) was measured using an inductive sensor (Kaman SMU 9000-15N). The resulting experimental input and output data was then used to obtain the system's model (\hat{P}_L). The piezopositioner used in these experiments was a 10 cm long sectored piezoelectric-tube actuator made of lead zirconate titanate (PZT).

2.2.1. Linearized model

The linearized dynamics (\hat{P}_L from Fig. 2) were modeled in transfer function form (\hat{P}_L) as

$$\hat{P}_L(s) = \frac{y}{u_{ff,L}} = k_L \frac{\prod_{m=1}^4 (s - z_{L,m})}{\prod_{n=1}^6 (s - p_{L,n})}, \quad (2)$$

where L denotes that the system is linearized (using charge control), $u_{ff,L}$ is the feedforward voltage input to the charge amplifier, k_L is the gain and $p_{L,n}$ and $z_{L,m}$ are the poles and zeros of the system. The gain for the model was found to be $k_L = 8.096 \times 10^6$ and the poles and zeros are given in Table 1.

Table 1
Zeros and poles of linearized model (\hat{P}_L in Eq. 2)

m and n	Zeros ($z_{L,m}$) (rad/s)	Poles ($p_{L,n}$) (rad/s)
1, 2	$-85.12 \pm 2530.93j$	$-33.43 \pm 1325.75j$
3, 4	$19505.41 \pm 33323.36j$	$-13533.10 \pm 3091.28j$
5, 6	-	$-278.73 \pm 19190.57j$

The frequency response of the transfer function model is compared to the experimental frequency response of the system obtained using the DSA in Fig. 6. As seen in the Figure, the model matches the experimental data well up to 4000 Hz.

2.2.2. Linear model without charge control

In order to contrast the feedforward-based positioning performance with and without the use of charge control to linearize the dynamics, the system was modeled without the charge amplifier, i.e., with a standard voltage amplifier, as shown in Fig. 7.

Although the dynamics are not linearized (as is the case with charge control), a frequency response (with the voltage amplifier) was obtained by keeping the positioner displacements significantly smaller than the maximum range of the positioner. For such small displacements, a linear model was obtained by fitting the experimental frequency response with a transfer function of the form

$$\hat{P}_N(s) = \frac{y}{u_{ff,N}} = k_N \frac{\prod_{m=1}^4 (s - z_{N,m})}{\prod_{n=1}^6 (s - p_{N,n})}, \quad (3)$$

where $u_{ff,N}$ is the feedforward voltage input to the voltage amplifier, with gain $k_N = 6.512 \times 10^6$ and poles and zeros as seen in Table 2 (the subscript N denotes that the system dynamics are not linearized with a charge amplifier).

The frequency responses of the transfer function model is compared to the experimental frequency response of the system obtained using the DSA in Fig. 8. As seen in the figure, the model adequately captures the system dynamics and the modeling errors (in the frequency response) are similar to the case with the charge amplifier in Fig. 6.

2.3. Inverse-feedforward

Given a desired output ($y = y_d$), the feedforward-input with the charge amplifier ($u_{ff,L}$ in Fig. 2) can be found by inverting the model of the system dynamics (\hat{P}_L)

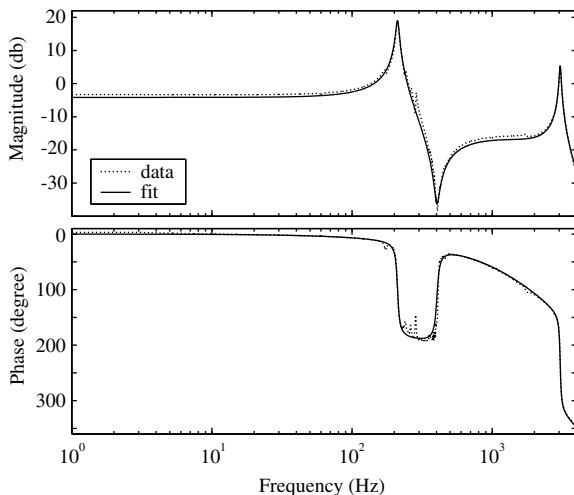


Fig. 6. Comparison of frequency response plots for the experimental system with charge control (dotted line) and the transfer function model (solid line).

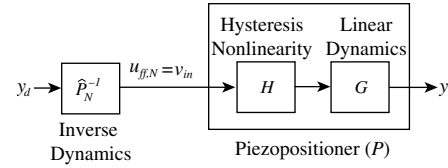


Fig. 7. Block diagram showing the feedforward control scheme for a voltage-controlled piezopositioner. The control scheme is similar to the charge-controlled case in Fig. 2, but without the charge amplifier.

Table 2
Voltage-controlled piezopositioner model zeros and poles

m and n	Zeros ($z_{N,m}$) (rad/s)	Poles ($p_{N,n}$) (rad/s)
1, 2	$-82.77 \pm 2535.17j$	$-32.06 \pm 1336.92j$
3, 4	$17376.26 \pm 33162.90j$	$-309.54 \pm 19189.82j$
5	–	-9666.62
6	–	-30669.86

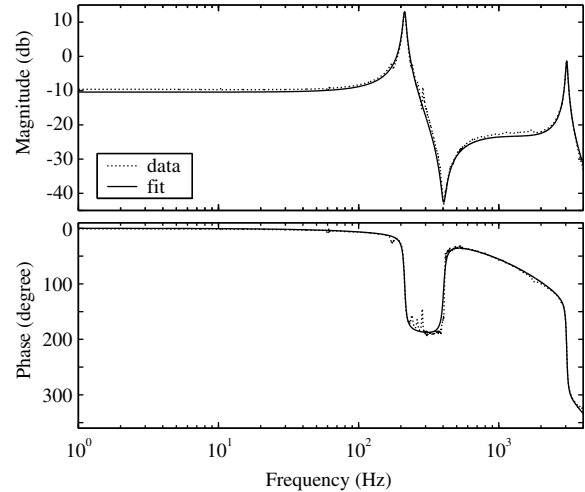


Fig. 8. Voltage control frequency response plots for the experimental system (dotted line) and the transfer function model (solid line).

$$u_{ff,L} = \hat{P}_L^{-1} y_d. \quad (4)$$

There are two issues in the computation of the feedforward-input with such an approach. First, this approach cannot account for design issues such as actuator saturation and bandwidth limitations. Second, the system model from Eq. (3) could be nonminimum phase (zeros of the system are the right-half of the complex plane), in which case the inverse system \hat{P}_L^{-1} will be unstable and standard approaches to compute the feedforward-input would lead to unbounded inputs. Both of these issues are discussed below.

2.3.1. Optimal inverse-feedforward

A Fourier-transform-based approach to compute bounded inverse inputs (even for nonminimum phase systems) was developed in [20]. This Fourier-based approach is extended by the optimal, inverse-feedforward method

[21], which enables trade-offs between input size and output-tracking precision. In particular, the inverse input is found by minimizing the following cost function:

$$J(u) = \int_{-\infty}^{\infty} \{u^*(j\omega)R(j\omega)u(j\omega) + [y(j\omega) - y_d(j\omega)]^*Q(j\omega)[y(j\omega) - y_d(j\omega)]\}d\omega, \quad (5)$$

where the terms are Fourier transforms of the input u , the achieved output y , the desired output y_d and $*$ denotes the complex conjugate transpose. The terms $R(j\omega)$ and $Q(j\omega)$ are real-valued frequency dependant weightings that penalize the input (u) and the tracking error ($y - y_d$) respectively. Both values should not be simultaneously zero at any frequency.

We point out two extreme cases for the choice of R and Q . First, if $Q = 0$ and R nonzero, then not tracking the desired trajectory would be the best approach ($u = 0$). In the second case, if $R = 0$ and Q is nonzero, then the best strategy is to track the desired scan path exactly ($y = y_d$). Note that in the second case, the input from the optimal inverse is the same as the input from the exact inverse, which allows the system to precisely track the desired output (at that particular frequency). Choice of R and Q in between these extreme cases allows for trade-off between minimization of vibrations and prevention of actuator saturation as discussed in Ref. [22].

By minimizing the cost function in Eq. 5 the optimal input (u_{opt}) can be found as

$$u_{\text{opt}}(j\omega) = \left[\frac{\hat{P}_L^*(j\omega)Q(j\omega)}{R(j\omega) + \hat{P}_L^*(j\omega)Q(j\omega)\hat{P}_L(j\omega)} \right] \times y_d(j\omega) \quad (6)$$

and the time-domain signal for the feedforward-input ($u_{\text{ff,L}}$) is then obtained through an inverse Fourier transform of $u_{\text{opt}}(j\omega)$ [21]. For the case without the charge control, the feedforward-input $u_{\text{ff,N}}$ is obtained using the same approach after substituting \hat{P}_N for \hat{P}_L in Eq. 6.

Remark: The time domain feedforward input (inverse Fourier transform of Eq. 6) is noncausal (but bounded) for nonminimum phase systems. Therefore, to implement this method for nonminimum phase systems, it is necessary to calculate the feedforward input offline and apply it to the system before the desired motion begins. For online implementation, a preview-based inversion method was developed in Refs. [23,24].

3. Experiments

Experimental results are used to show that the ability of charge control to linearize the piezopositioner enables the use of linear inverse-feedforward, which can substantially reduce positioning error.

3.1. Design of experiments

To evaluate the capabilities of inverse-feedforward with charge control, output-tracking of a desired trajectory (y_d) of three cases are compared experimentally:

1. Linear inverse-feedforward with charge control,
2. linear inverse-feedforward without charge control (i.e., with the voltage amplifier), and
3. DC-gain control (without charge control), where the feedforward input is calculated without considering the vibrational dynamics, i.e., based on the low-frequency gain (DC-gain) as

$$u_{\text{ff,DC}} = \frac{y_d}{\text{DC}_{\text{Gain}}}. \quad (7)$$

The desired trajectory was chosen as a filtered $\pm 2 \mu\text{m}$ triangular output trajectory (y_d); the filter was chosen such that the first three components of the triangular waves Fourier expansion were below the filter's cutoff frequency.

Remark: It is impossible to track a pure triangular trajectory with finite inputs since the acceleration at the

Table 3
Weighting factors (R and Q) at different frequencies in Eq. (5)

Frequency (Hz)	0	150	250	275	500	525	1800	2000
Q	1	1	1	0	0	1	1	0
R	0	0	0	1	1	0	0	1

Weights at intermediate frequencies were obtained using linear interpolation.

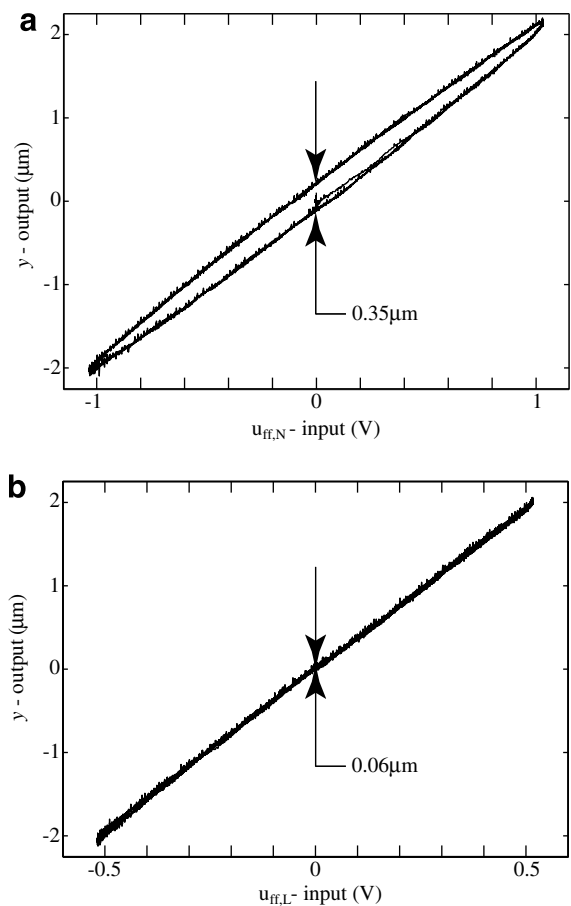


Fig. 9. Experimental hysteresis loops for a 10 Hz desired output of $\pm 2 \mu\text{m}$. (a) Without charge control and (b) with charge control.

turnarounds is unbounded. Thus the desired trajectory is chosen to be a filtered, triangle-like trajectory to assure bounded accelerations and therefore, bounded inputs.

3.2. Experimental methods

3.2.1. Isolating the feedforward performance

To isolate the effects of the feedforward-input, the following experiments are carried out using open loop control. In general, feedforward is used in conjunction with a feedback controller, e.g. [3,12,25–28]; feedforward in conjunction with feedback tends to improve the tracking performance when compared to the use of feedback alone [2]. However, in this study, we focus on the use of feedforward alone (without feedback) to isolate and investigate the effects of charge control on the inverse-feedforward approach.

3.2.2. Weighting factors in optimal inverse

The inverse-feedforward-input was computed using the optimal inverse-feedforward method (described in Section 2.3.1). The choice of the weighting factors (R and Q in Eq. 5) are shown in Table 3.

At frequencies where we seek perfect tracking we set the weight on the tracking error to be high ($Q = 1$) relative to the weight on the input ($R = 0$). At high frequencies, the gain of the system is small (see Fig. 6) – therefore, large inputs are needed to track output signals at such frequen-

cies. To avoid actuator saturation we do not seek to track at relatively high frequencies beyond 2000 Hz, i.e., we choose $Q = 0$ and $R = 1$. Similarly, we do not seek to track in the region where the system gain is small due to the presence of the zeros (see Fig. 6), i.e., we again set $Q = 0$ and $R = 1$ in the frequency interval 275–500 Hz. Thus, the choice of the weights (Q, R) allows trade-offs between the tracking precision and the input size.

3.2.3. Positioning error quantification

The results were quantified in terms of the output-tracking error using percentage root-mean-square (RMS) error,

$$e_{\text{rms},\%} = \left[\left(\sqrt{\frac{\sum_{i=1}^n (y_i - y_{d,i})^2}{n}} \right) / y_{d,\text{max}} \right] \times 100, \quad (8)$$

where y is the actual output from the system and n is the number of sample points, and the maximum percentage error

$$e_{\text{max},\%} = [\max(y_i - y_{d,i}) / y_{d,\text{max}}] \times 100, \quad (9)$$

where $y_{d,\text{max}}$ represents the maximum desired displacement ($2 \mu\text{m}$).

3.3. Charge control linearizes the piezopositioner

The use of charge control linearizes the overall dynamics of the piezopositioner. The amount of hysteresis reduction

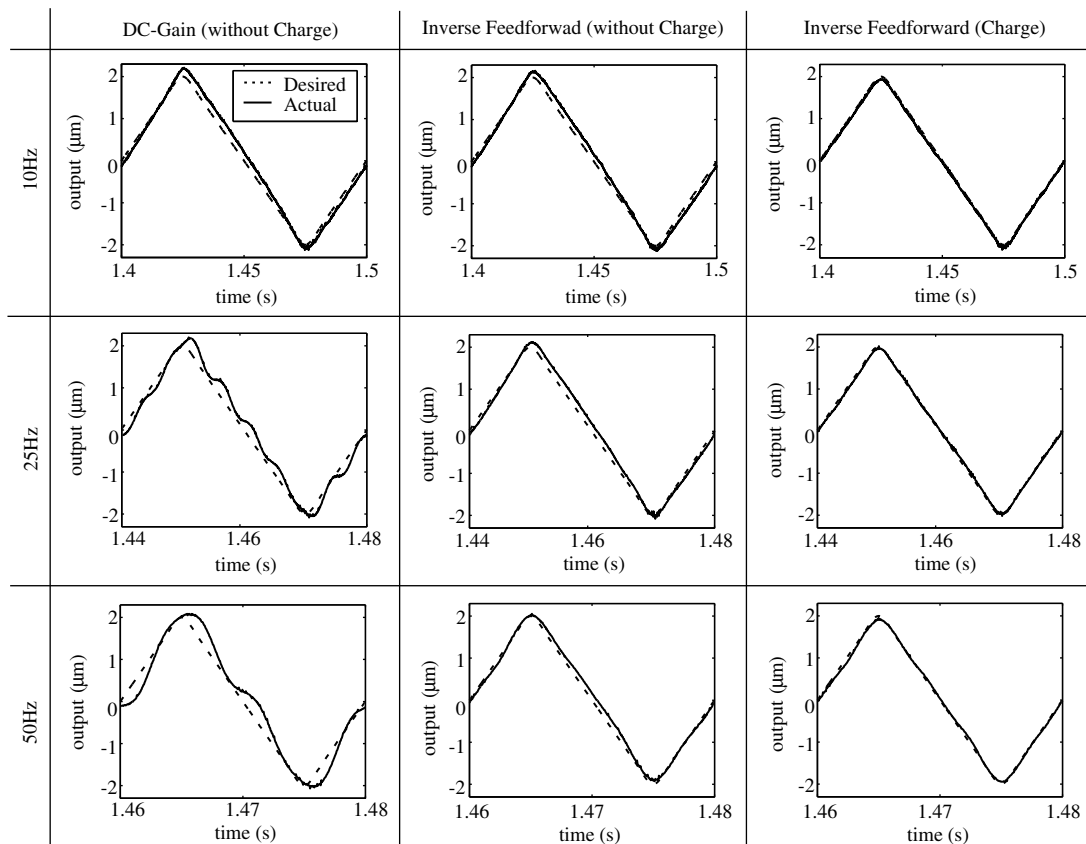


Fig. 10. Experimental output plots for different control techniques (DC-Gain, inverse-feedforward without charge control, and inverse-feedforward with charge control) at different frequencies (10, 25, and 50 Hz).

afforded by charge control can be shown by plotting the input versus output for both cases: with charge control and without charge control as shown in Fig. 9 for 10 Hz, which is in the charge control region of the amplifier since the crossover frequency (ω_c) between voltage amplifier and charge amplifier, is $f_c = \omega_c/2\pi = 1/2\pi R_s C_s = 0.04$ Hz. Note that the input axes are on different scales due to the difference in amplifier gain between the voltage and charge amplifiers (see Figs. 6 and 8). Fig. 9a shows the hysteresis loop for the case without charge control (block diagram shown in Fig. 7), while Fig. 9b shows the loop for the charge control case (block diagram shown in Fig. 2). The amount of hysteresis reduction is quantified by determining the maximum output deviation at zero input (shown between the arrows). Without charge control, the hysteresis loop is approximately $0.35 \mu\text{m}$ wide (8.8% of the maximum desired displacement) compared to $0.06 \mu\text{m}$ (1.5%) when charge control is used, a reduction in hysteresis of 83%. Thus, charge control reduces hysteresis significantly—essentially linearizing the system.

3.4. Inverse-feedforward with charge control improves output-tracking

The use of charge control, which linearizes the piezopositioner, enables the use of linear inverse-feedforward.

In piezopositioners, positioning errors come from two primary sources: (1) hysteresis and (2) vibrations, both of which can be seen when using the DC-Gain method (Figs. 10 and 11 column 1 and Table 4 column 1). First, hysteresis exists at all frequencies, but tends to dominate the positioning error at low frequencies because the vibrational errors are small. It manifests itself as a lag-like behavior in the output, as can be seen in the 10 Hz DC-Gain plot shown in Fig. 10 (column 1, row 1). Second, vibrations tends to increase as the operating frequency approaches the first system resonance (in this case 210 Hz), as can be seen in the DC-Gain column of Fig. 10 (column 1).

Both hysteresis and vibrations can be overcome by using inverse-feedforward with charge control. This can be seen by comparing the Inverse-Feedforward (Charge) and DC-Gain (without Charge) columns of Fig. 10 (columns 1 and 3). At 10 Hz the error seen in the DC-Gain method (primarily caused by hysteresis) is significantly reduced when inverse-feedforward with charge control is used (RMS error is reduced from 3.0% to 1.0% (67% reduction) – as seen in Table 4). As the frequency is increased to 50 Hz, vibrational error, seen in the DC-Gain method, is also reduced when inverse-feedforward with charge control is used (RMS error is reduced from 5.0% to 1.1% (78% reduction)).

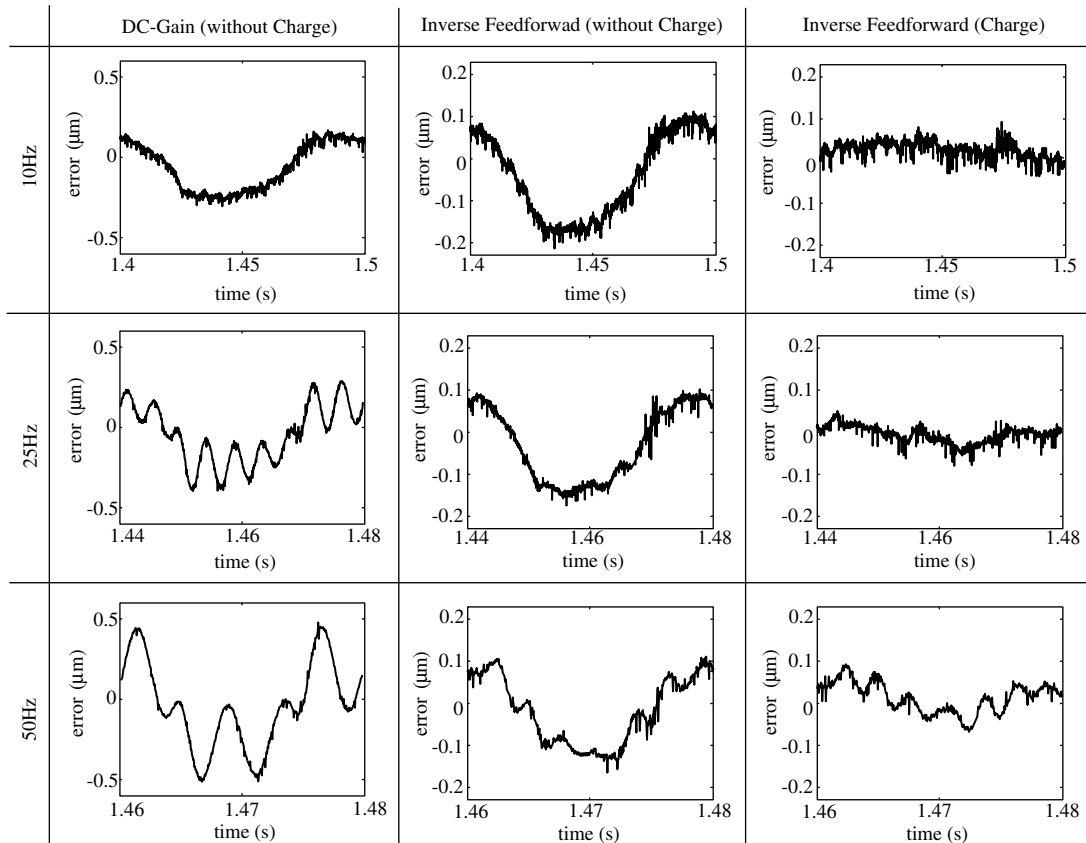


Fig. 11. Experimental error plots ($y_d - y$) for different control techniques (DC-Gain, inverse-feedforward without charge control, and inverse-feedforward with charge control) at different frequencies (10, 25, and 50 Hz).

Table 4
Error data at various frequencies

f (Hz)	DC-Gain ($e_{rms,\%}/e_{max,\%}$)	Inverse-feedforward voltage ($e_{rms,\%}/e_{max,\%}$)	Inverse-feedforward charge ($e_{rms,\%}/e_{max,\%}$)
10	3.0/15.3	2.7/14.0	1.0/5.6
25	3.4/20.1	2.4/12.7	0.9/5.4
50	5.0/30.3	2.2/12.1	1.1/8.1
75	24.6/109.3	2.3/13.5	1.6/9.2

3.5. Comparison of inverse-feedforward with and without charge control

The tracking performance of inverse-feedforward, with and without charge control, are compared in Figs. 10 and 11 and Table 4 (columns 2 and 3 in all). The inverse-feedforward of a linear model, without charge control, reduces vibrational errors but not hysteresis effects. In contrast, the use of charge control allows reduction of the hysteresis and vibration effects in a piezopositioner with the inverse of a linear model. This is because the overall system dynamics, which include the charge amplifier, are linear. For example, at 10, 25, and 50 Hz, the RMS error reduced from 2.7% to 1.0% (63% reduction), 2.4% to 0.9% (63% reduction) and 2.2% to 1.1% (50% reduction) respectively as seen in Figs. 10 and 11. Thus, the use of charge control to linearize the system, substantially improves the performance of linear inverse-feedforward.

3.6. Trade-off between tracking accuracy and input magnitude

The use of an optimal inverse allows trade-off between tracking accuracy and input magnitude. For example, consider the tracking results for a 75 Hz output shown in Fig. 12 – the data is quantified in Table 4 (row 4). As before, the use of the inverse-feedforward substantially reduces

the tracking error (93% error reduction when compared to DC-Gain without charge control). However, the residual tracking error has a significant 375 Hz component as seen in Fig. 12 (column 2 and 3, row 2) – the error has five cycles in each 75 Hz period. Note that 375 Hz is the third component in the Fourier expansion of the 75 Hz triangular output-trajectory. We expect to see positioning error at this frequency when the optimal inverse-feedforward-input is used. This is because the optimal inverse was designed to not track the 375 Hz frequency component, which lies in the untracked frequency range (275–500 Hz), see discussion in Section 3.2.2.

The residual error at 375 Hz could have been corrected, but at the cost of greater input magnitude. The input required for such removal of the residual error at 375 Hz is computed by changing the cost function to achieve full tracking and the resulting full-inverse input is shown in Fig. 13. Note that the full-inverse input (center plot in Fig. 13) is substantially larger than the optimal input (first plot in Fig. 13) – magnitude of 0.75 V when compared to the optimal inverse magnitude of 0.48 V which is a 56% increase in the maximum input needed. When applied to the piezopositioner, this large increase in the input magnitude (almost doubling) would only result in a small decrease in output error (maximum output error is 0.18 μm or 9% of the maximum desired output, 2 μm). The need for such large input arises because the gain of

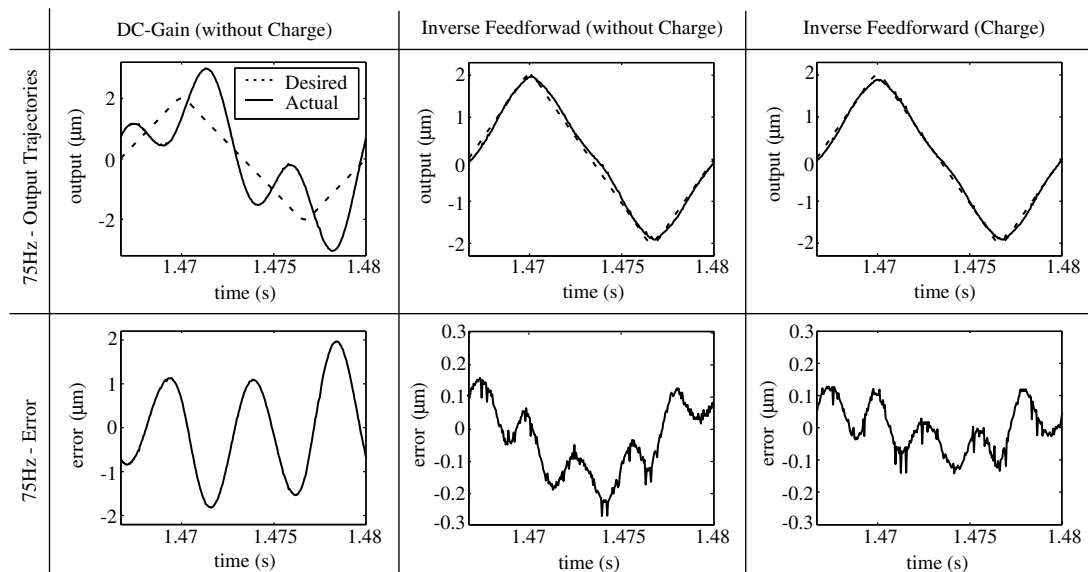


Fig. 12. Experimental output and error ($y_d - y$) plots for different control techniques (DC-Gain, inverse-feedforward without charge control, and inverse-feedforward with charge control) at 75 Hz.

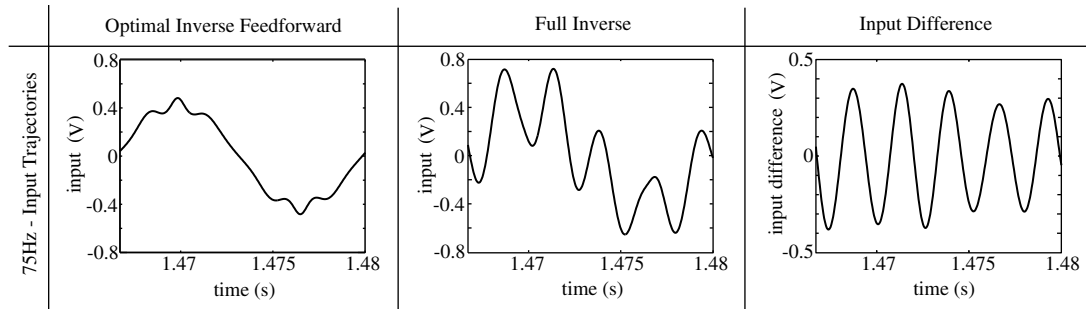


Fig. 13. Experimental input plots for inverse-feedforward (charge) at 75 Hz, showing, from right to left, the input calculated using the optimal inverse scheme, the input calculated using the full-inverse, and the difference in the two inputs.

the system at 375 Hz is small as it is close to the system zero (see Fig. 6). The advantage of the optimal inversion approach is that it allows the designer to trade-off this relatively small improvement in output-tracking accuracy for a substantially reduced feedforward-input magnitude.

4. Conclusion

This article addressed problems associated with the inverse-feedforward control of piezopositioners. The main contribution was to negate the necessity to invert the complex hysteresis nonlinearity by first linearizing the piezopositioner using charge control, and then applying linear inverse-feedforward to this system. This method was experimentally verified using a piezoelectric-tube actuator and the advantages were shown by comparing the positioning performance with and without the use of charge control. For example, at an operating frequency of 50 Hz, the linear inverse-feedforward with charge control could reduce the tracking error by 50% when compared to the case without charge control.

References

- [1] Croft D, Shedd G, Devasia S. Creep, hysteresis, and vibration compensation for piezoactuators: atomic force microscopy application. *ASME J Dyn Syst Measure Contr* 2001;123:35–43.
- [2] Devasia S. Should model-based inverse inputs be used as feedforward under plant uncertainty? *IEEE T Automat Contr* 2002;47(11):1865–71.
- [3] Leang KK, Devasia S. Feedback-linearized inverse feedforward for creep, hysteresis, and vibration compensation in piezoactuators. *IEEE T on Contr Syst T: Special Issue on Dynamics and Control of Micro and Nano-scale Systems* 2007; In Press.
- [4] Binnig G, Smith DPE. Single-tube three-dimensional scanner for scanning tunneling microscopy. *Rev Sci Instrum* 1986;57(8):1688–9.
- [5] Quate CF. Scanning probes as a lithography tool for nanostructures. *Surf Sci* 1997;386:259–64.
- [6] Newcomb CV, Flinn I. Improving the linearity of piezoelectric ceramic actuators. *IEE Electron Lett* 1982;18(11):442–3.
- [7] Fleming AJ, Moheimani SOR. Sensorless vibration suppression and scan compensation for piezoelectric-tube nanopositioners. *IEEE T Contr Syst T* 2006;14(1):33–44.
- [8] Ge P, Jouaneh M. Tracking control of a piezoceramic actuator. *IEEE T Contr Syst T* 1996;4(3):209–16.
- [9] Song D, Li CJ. Modeling of piezo actuator's nonlinear and frequency dependent dynamics. *Mechatron Sci Intell Mach* 1999;9(4):391–410.
- [10] Hu H, Ben-Mrad R. On the classical Preisach model for hysteresis in piezoceramic actuators. *Mechatron Sci Intell Mach* 2003;13(2):85–94.
- [11] Janocha H, Kuhn K. Real-time compensation of hysteresis and creep in piezoelectric actuators. *Sensor Actuat A* 2000;79:83–9.
- [12] Choi GS, Lim YA, Choi GH. Tracking position control of piezoelectric actuators for periodic reference inputs. *Mechatron Sci Intell Mach* 2002;12(5):669–84.
- [13] Jung SB, Kim SW. Improvement of scanning accuracy of PZT piezoelectric actuators by feed-forward model-reference control. *Precis Eng* 1994;17:49–55.
- [14] Croft D, Devasia S. Hysteresis and vibration compensation for piezoactuators. *J Guid Control Dyn* 1998;21(5):710–7.
- [15] Croft D, Devasia S. Vibration compensation for high-speed scanning tunneling microscopy. *Rev Sci Instrum* 1999;70(12):4600–5.
- [16] Schitter G, Stemmer A. Model-based signal conditioning for high-speed atomic force and friction force microscopy. *Microelectron Eng* 2003;67–68:938–44.
- [17] Goldfarb M, Celenovic N. A lumped parameter electromechanical model for describing the nonlinear behavior of piezoelectric actuators. *J Dyn Syst* 1997;119:478–85.
- [18] Moheimani SOR, Vautier BJG. Resonant control of structural vibration using charge-driven piezoelectric actuators. *IEEE T Contr Syst T* 2005;13(6):1021–35.
- [19] Yi KA, Veillette RJ. A charge controller for linear operation of a piezoelectric stack actuator. *IEEE T Contr Syst T* 2005;13(4):517–26.
- [20] Bayo E. A finite-element approach to control the end-point motion of a single link flexible robot. *J Robot Syst* 1987;4:63–74.
- [21] Dewey JS, Leang K, Devasia S. Experimental and theoretical results in output-trajectory redesign for flexible structures. *ASME J Dyn Syst Measure Contr* 1998;120:456–61.
- [22] Brinkerhoff R, Devasia S. Output-tracking for actuator deficient/redundant systems: multiple piezoactuator example. *J Guid Control Dyn* 1999;23(2):370–3.
- [23] Zou Q, Devasia S. Preview-based stable-inversion for output tracking of linear systems. *ASME J Dyn Syst Measure Contr* 1999;121(4):625–30.
- [24] Zou Q, Devasia S. Preview-based optimal inversion for output tracking: application to scanning tunneling microscopy. *IEEE T Contr Syst T* 2004;12(3):375–86.
- [25] Kouno E. A fast response piezoelectric actuator for servo correction of systematic errors in precision machining. *Ann CIRP* 1982;33(1):369–72.
- [26] Sebastian A, Salapaka SM. Design methodologies for robust nanopositioning. *IEEE T Contr Syst T* 2005;13(6):868–76.
- [27] Lin CJ, Yen SR. Precise positioning of piezo-actuated stages using hysteresis-observer based control. *Mechatron Sci Intell Mach* 2006;16(7):417–26.
- [28] Crudele M, Kurfess TR. Implementation of a fast tool servo with repetitive control for diamond turning. *Mechatron Sci Intell Mach* 2003;13(3):243–57.